



Changes in the partial pressure of carbon dioxide in the Mauritanian–Cap Vert upwelling region between 2005 and 2012

Melchor González-Dávila¹, J. Magdalena Santana Casiano¹, and Francisco Machín^{1,2}

¹Instituto de Oceanografía y Cambio Global, Grupo QUIMA, Universidad de Las Palmas de Gran Canaria, 35017, Las Palmas de Gran Canaria, Spain

²Departamento de Física, Universidad de Las Palmas de Gran Canaria, 35017, Las Palmas de Gran Canaria, Spain

Correspondence to: Melchor González-Dávila (melchor.gonzalez@ulpgc.es)

Received: 9 March 2017 – Discussion started: 29 March 2017

Revised: 26 July 2017 – Accepted: 28 July 2017 – Published: 31 August 2017

Abstract. Coastal upwellings along the eastern margins of major ocean basins represent regions of large ecological and economic importance due to the high biological productivity. The role of these regions for the global carbon cycle makes them essential in addressing climate change. The physical forcing of upwelling processes that favor production in these areas are already being affected by global warming, which will modify the intensity of upwelling and, consequently, the carbon dioxide cycle. Here, we present monthly high-resolution surface experimental data for temperature and partial pressure of carbon dioxide in one of the four most important upwelling regions of the planet, the Mauritanian–Cap Vert upwelling region, from 2005 to 2012. This data set provides direct evidence of seasonal and inter-annual changes in the physical and biochemical processes. Specifically, we show an upwelling intensification and an increase of 0.6 Tg yr^{-1} in CO_2 outgassing due to increased wind speed, despite increased primary productivity. This increase in CO_2 outgassing together with the observed decrease in sea surface temperature at the location of the Mauritanian Cap Blanc, 21°N , produced a pH rate decrease of $-0.003 \pm 0.001 \text{ yr}^{-1}$.

and temporal observations representative of the distribution of CO_2 fluxes between the ocean and atmosphere are necessary. Automated instruments on volunteer observing ships (VOSs) serve to provide as many observations throughout the global ocean as possible. This is in addition to data collected on scientific cruises and at long-term moorings (i.e., Astor et al., 2005; Lüger et al., 2004, 2006; González-Dávila et al., 2005, 2009; Schuster et al., 2009; Ullman et al., 2009; Watson et al., 2009; Padin et al., 2010; Gruber et al., 2002; Dore et al., 2003; Santana-Casiano et al., 2007; Bates et al., 2014).

With the amount of data already gathered (<http://www.socat.info/>; Pfeil et al., 2013), climatologies that present average CO_2 fluxes between the atmosphere and the ocean have been developed, identifying areas acting as a source or sink (Key et al., 2004; Takahashi et al., 2009). However, the low spatial resolution of these databases limits the applicability, especially in coastal areas. Upwelling regions are particularly under-represented in such large databases. Upwelling presents a dynamic process that raises nutrient and CO_2 -rich water from relatively deep areas to the surface. The nutrients reaching the photic zone promote primary production, which consumes CO_2 . This process generates a CO_2 flux into the ocean. On the other hand, upwelling also brings up CO_2 from deep seawater, which generates uncertainty about the actual role of upwelling areas as a source or sink of CO_2 (Michaels et al., 2001). Indeed, upwelling areas may act as a source or sink of CO_2 depending on their location (Cai et al., 2006; Chen et al., 2013), where upwelling regions at low latitudes mainly act as a source of CO_2 (Feely et al., 2002; Astor et al., 2005; Friederich et al., 2008; Santana-Casiano et al., 2009; González-Dávila et al., 2009) and those at midlatitudes

1 Introduction

The excess of CO_2 in the atmosphere, largely responsible for global climate change, has prompted research on the role of the oceans in the carbon cycle. The aim in recent decades has been to assess how the oceans act as sources or sinks within the carbon cycle. To achieve this goal, highly resolved spatial

mainly act as a sink of CO_2 (Frankignoulle and Borges, 2001; Hales et al., 2005; Borges and Frankignoulle, 2002; Borges et al., 2005; Santana-Casiano et al., 2009; González-Dávila et al., 2009). Several anthropogenic interactive effects strongly influence eastern boundary upwelling systems (EBUSs), including upper ocean warming, ocean acidification, and ocean deoxygenation (Gruber, 2011; Feely et al., 2008; Keeling et al., 2010). Moreover, evidence of increasing wind speed that would favor upwelling (Bakun, 1990; Demarcq, 2009; Oerder et al., 2015) supports the possibility of a change in the dynamics of these highly productive areas. Recently, eddy-resolving regional ocean models have shown how upwelling intensification can cause a major impact on the system's biological productivity and CO_2 outgassing (Lachkar and Gruber, 2013; Oerder et al., 2015). Wind observations and re-analysis products are controversial regarding the Bakun intensification hypothesis (Bakun, 1990). Using different wind databases for the Canary region, Barton et al. (2013) concluded that there was no evidence for a general increase in the upwelling intensity off northwest Africa. Marcello et al. (2011) found an intensification of the upwelling system in the same area during a 20-year period, while the alongshore wind stress remained almost stable. Cropper et al. (2014) found that coastal summer wind speed increased, resulting in an increase in upwelling-favorable wind speeds north of 20°N and an increase in downwelling-favorable winds south of 20°N . Santos et al. (2005, 2012) showed that sea surface temperature (SST) was not homogeneous either along latitude or longitude and depended on the upwelling index (UI) intensity. Varela et al. (2015) demonstrated opposite results worldwide depending on the length of data, season evaluated, and selected area within the same wind data set or between data sets. For the Mauritanian region, when wind stress data were used (Varela et al., 2015), a more persistent increasing trend in upwelling-favorable winds north of 21°N and a decreasing trend south of 19°N was determined.

Starting in June 2005, the QUIMA-VOS line visited the Mauritanian–Cap Vert upwelling region northwest of Africa on a monthly basis (Fig. 1 and Table S1 in the Supplement) producing for the first time a high-resolution database of SST and partial pressure of CO_2 expressed as fugacity $f\text{CO}_2$. This database shows the variations in the CO_2 system under changes in the upwelling conditions in the Canary ecosystem from 27 to 10°N for the period 2005 to 2012. More data for the region from other surveys exist (<http://www.socat.info/>; Pfeil et al., 2013) but they were not considered in this study as they do not follow the same track as the QUIMA-VOS line. Those data are strongly influenced by the distance to the upwelling cells with the corresponding physical effects in the partial pressure of CO_2 .

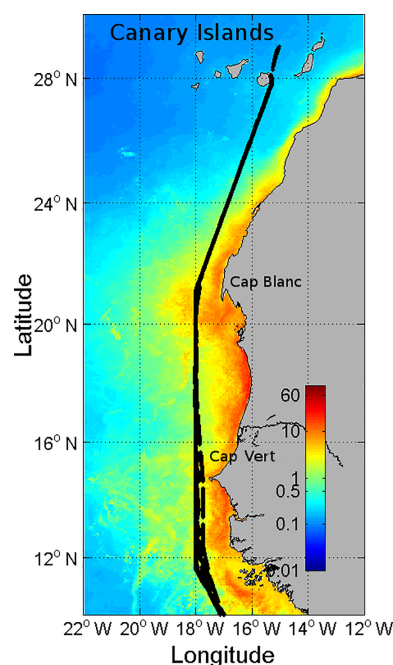


Figure 1. Ship track (black line) in the area from 28°N (Gran Canaria, the Canary Islands) to 10°N . The locations of Cap Blanc and Cap Vert are indicated. Monthly OceanColor Web (<https://oceancolor.gsfc.nasa.gov/>) data for average chlorophyll *a* concentration (mg m^{-3}) were included in a MATLAB routine and annually averaged. The map has been generated using MATLAB 7.12 R2011a.

2 Experimental

2.1 Study region

The VOS line crosses the east Atlantic Ocean from the north of Europe (English Channel) to South Africa, calling at Gran Canaria, the Canary Islands, with a periodicity of 2 months, which provides monthly data (southward or northward sections). In this work, the area between Gran Canaria at 27 and 10°N has been selected in order to study the Mauritanian–Cap Vert upwelling region. On its route south (Fig. 1), the ship leaves Gran Canaria and goes straight to 100 km off Cap Blanc at 21°N , $17^\circ 45' \text{W}$. It then follows this longitude, passing at 100 km off Cap Vert until 12°N , where it changes direction to Cape Town, reaching 10°N , 17°W at 330 km off the coast of Guinea. Between 22 and 20°N , the ship reaches the 500 m isobath. South of 15°N , the ship moves between the 1000 and 500 m isobaths. On its route north, the ship follows the reverse track.

2.2 Experimental data

Experimental data were obtained under the EU projects CARBOOCEAN and CARBOCHANGE (www.CarboOcean.org and <https://carbochange.b.uib.no/>) and now also available at <http://www.socat.info/> (Pfeil et al.,

2013). An autonomous instrument for the determination of the partial pressure of CO₂ developed by Craig Neill following NOAA recommendations was installed on a VOS line. This was operated by the Mediterranean Shipping Company S.A. from 2005 to 2008 and Maersk from 2010 to 2012. This VOS line (QUIMA-VOS) ran between the UK and Cape Town from July 2005 to January 2013 (Table S1 in the Supplement). Temperature was measured at three positions along the sampling circuit: in the intake (Sea-Bird SBE38L), in the equilibrator (Sea-Bird thermosalinograph SBE21 and internal PT100 thermometer), and in the oxygen sensor (Optode 3835, AanderaaTM). After the seawater pump, the intake is divided into two lines, one feeding the CO₂ system and the other feeding the oxygen sensor, the fluorometer, and the Sea-Bird thermosalinometer. Differences between equilibrator and intake temperatures were constant in time due to the high seawater flow but varied among ships due to the different locations of the equipment. Values varied between 0.06 °C when the equipment was placed close to the intake and 0.35 °C when the equipment was one floor above and inside the engine room. The SST was also obtained from the NOAA_OI_SST-V2 data provided by the NOAA/OAR/ESRL PSD from Boulder, Colorado, USA (<http://www.esrl.noaa.gov/psd>). These data had a spatial resolution of 1° latitude and 1° longitude and monthly averages were used. The correlation between our experimental SST data and satellite data was better than ±1 °C, and improved to ±0.4 °C after removing the most affected upwelling regions (19–22 and 14–16° N), which related to the high variability imposed by the upwelling.

The CO₂ molar fraction, $x\text{CO}_2$, was obtained every 150 s in seawater, while atmospheric $x\text{CO}_2$ data were obtained every 180 min. The seawater intake was located at a 10 m depth. The system was calibrated every 3 hours by measuring four different standard gases with mixing ratios in the ranges of 0.0, 250–290, 380–410, and 490–530 ppm of CO₂ in the air, provided by NOAA and traceable to the World Meteorological Organization scale. The precision of the system is greater than 0.5 µatm and the accuracy estimated with respect to the standard gases is of 1 µatm inside the standards' range. For $x\text{CO}_2$ values higher than the highest standard (532.04 ppm), the accuracy will be reduced, even when linearity was observed in all cases inside the standards range. The fugacity of CO₂ ($f\text{CO}_2$, µatm) was calculated from $x\text{CO}_2$ after correcting for temperature differences between intake and equilibrator, according to the expressions for seawater given by DOE (1994). Normalized $f\text{CO}_2$ ($Nf\text{CO}_2$) derived from the mean SST for the area (T_{mean}) was computed following Takahashi et al. (1993) as

$$(Nf\text{CO}_2) = f\text{CO}_2 \cdot \exp[0.0423 (T_{\text{mean}} - \text{SST})]. \quad (1)$$

In order to compute a second carbonate system variable, the surface total alkalinity (A_T) was computed from sea surface salinity (SSS) and SST (Lee et al., 2006). pH_T at the in situ

temperature was computed from $f\text{CO}_2$ and A_T and with average annual surface ocean total phosphate and total silicate concentrations of 0.5 and 4.8 µmol kg⁻¹, respectively, from the World Ocean Atlas 2009, using the carbonic acid acidity constants by Mehrbach et al. (1973) refitted by Dickson and Millero (1987).

Air–sea CO₂ fluxes (FCO_2 , mmol m⁻² d⁻¹) were evaluated as

$$\text{FCO}_2 = 0.24 \cdot k \cdot s \cdot (f\text{CO}_2^{\text{sw}} - f\text{CO}_2^{\text{atm}}), \quad (2)$$

where 0.24 is the scale factor, k is the gas transfer velocity, s is the CO₂ solubility, $f\text{CO}_2^{\text{sw}}$ is the seawater fugacity of CO₂, and $f\text{CO}_2^{\text{atm}}$ is the atmospheric fugacity of CO₂. In order to evaluate $(f\text{CO}_2^{\text{sw}} - f\text{CO}_2^{\text{atm}})$, $f\text{CO}_2^{\text{atm}}$ data were linearly interpolated to the $f\text{CO}_2^{\text{sw}}$ time vector. A positive value for FCO_2 corresponds to CO₂ outgassing from the ocean. k (cm h⁻¹) was evaluated with the following parameterization (Nightingale et al., 2000):

$$k = (0.222 \cdot W^2 + 0.333 \cdot w) \cdot (Sc/660)^{-1/2}, \quad (3)$$

where W is the wind speed at 10 m above the sea surface (m s⁻¹) and Sc is the Schmidt number.

The variables involved in estimating FCO_2 data (i.e., $f\text{CO}_2^{\text{sw}}$, $f\text{CO}_2^{\text{atm}}$, SST, and SSS) were fitted to sinusoidal expressions (Lüger et al., 2004) for a given latitude as follows:

$$X(\text{lat})^* = a_0 + a_1(t - 2005) + a_2 \sin(2\pi t) + a_3 \cos(2\pi t) + a_4 \sin(4\pi t) + a_5 \cos(4\pi t), \quad (4)$$

where a_i are the fitting coefficients, t is the sampling time expressed as year fraction, and $X(\text{lat})^*$ represents any of the four fitted variables. This procedure allowed us to reconstruct the series of experimental data for periods without monthly data. The variables were decomposed into an interannual term $X(\text{lat})_i^* = a_0 + a_1(t - 2005)$ plus a periodical term $X(\text{lat})_p^* = a_2 \sin(2\pi t) + a_3 \cos(2\pi t) + a_4 \sin(4\pi t) + a_5 \cos(4\pi t)$, that is, $X(\text{lat})^* = X(\text{lat})_i^* + X(\text{lat})_p^*$. The periodical term accounts for the high-frequency seasonal variability, while the interannual term marks the year-to-year trend. First, observations were grouped in a natural year for a given latitude, as if they had been taken in a single year (no correction was done for interannual variability). The mean seasonal climatology data associated with the periodic coefficients (i.e., a_2 , a_3 , a_4 , and a_5) throughout the sampling period were determined. Next, the interannual coefficient a_1 was calculated by fitting the residuals resulting from subtracting the periodical component, $X(\text{lat})_p^*$, from the original variable $X(\text{lat})$. By fixing these five coefficients (a_1 – a_5), new distributions for $f\text{CO}_2^{\text{sw}*}$, $f\text{CO}_2^{\text{atm}*}$, SST*, and SSS* were constructed with a daily resolution based on the curve fits given for each variable as in Eq. (4), providing the coefficient a_0 . The accuracy of this fitting procedure was checked by both computing the correlation between experimental and reconstructed values and by determining the mean residuals. The Pearson coefficients were always over 0.87 for

SST (average 0.94 ± 0.03), over 0.69 for both $f\text{CO}_2^{\text{sw}}$ and $f\text{CO}_2^{\text{atm}}$ (average of 0.79 ± 0.07 and 0.82 ± 0.04 , respectively), and over 0.67 for SSS (average 0.79 ± 0.07). The mean residual on the determination of those four variables were $\pm 3.7 \mu\text{atm}$, $\pm 1.5 \mu\text{atm}$, $\pm 0.22^\circ\text{C}$, and ± 0.05 for $f\text{CO}_2^{\text{sw}*}$, $f\text{CO}_2^{\text{atm}*}$, SST^* , and SSS^* , respectively. When the monthly satellite SST values were considered, the new SST^* function averaged for each month produced values within $\pm 0.47^\circ\text{C}$, confirming that this procedure was able to fit non-sampled periods. It was assumed that the same procedure was valid for non-sampled $f\text{CO}_2$. Finally, daily FCO_2^* time series between 10 and 27°N with a latitudinal resolution of 0.5° were calculated with a standard error of estimation of $0.5 \text{ mmol m}^{-2} \text{ d}^{-1}$ (15 % of error) that produced mean residuals (experimental $\text{FCO}_2 - \text{FCO}_2^*$) of $0.4 \text{ mmol m}^{-2} \text{ d}^{-1}$ and Pearson correlation coefficients between experimental and computed FCO_2^* of $r > 0.6$, $p < 0.01$.

Chlorophyll *a* was calculated from measurements made by the Moderate-resolution Imaging Spectroradiometer (MODIS) aboard NASA's Aqua satellite. We used monthly averages with a spatial resolution of 9 km supplied by Ocean-Color Web (<https://oceancolor.gsfc.nasa.gov>).

Wind data were downloaded from the NCEP CFSR database at <http://rda.ucar.edu/pub/cfsr.html> developed by NOAA and retrieved from the NOAA National Operational Model Archive and Distribution System and maintained by the NOAA National Climatic Data Center. The spatial resolution is approximately $0.3 \times 0.3^\circ$ and the temporal resolution is 6 h. The reference height for the wind data is 10 m.

Rainfall data were collected by the precipitation radar installed on the Tropical Rainfall Measuring Mission (TRMM) satellite (<http://precip.gsfc.nasa.gov>). Monthly averages with a spatial resolution of $0.5 \times 0.5^\circ$ (product 3A12, version 07) were used (Fig. S1 in the Supplement) in order to explain changes in seasonal surface salinity distributions.

3 Results and discussion

3.1 Physical properties

The variability of the Mauritanian–Cap Vert upwelling was analyzed in terms of the upwelling index (Nykjaer and Van Camp, 1994) (Fig. 2) using satellite wind data. Negative UI values correspond to upwelling-favorable conditions and positive values to downwelling-favorable conditions. The lowest negative values of the index correspond to more intense upwelling. Results clearly distinguish two main subareas in the upwelling system: (1) north of 20°N , the upwelling conditions were favorable throughout the year, although the highest upwellings were observed from March to September with a northward shift from 20 to 22°N . (2) South of 20°N , a marked seasonality was observed with favorable upwelling conditions during autumn and winter, with the maximum intensity observed during January and February. In this

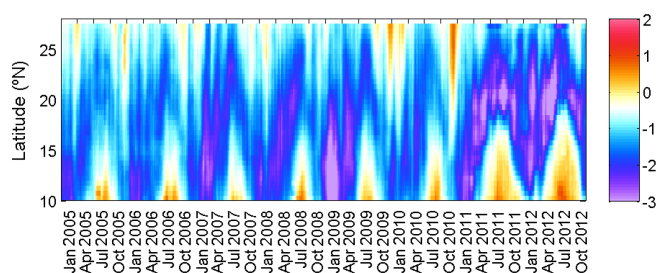


Figure 2. Time series of upwelling index (UI, $\times 10^{-3} \text{ m}^2 \text{ s}^{-1}$) in the Mauritanian–Cap Vert upwelling region along the ship track computed following Nykjaer and Van Camp (1994). Blue colors are related to upwelling events and red colors to downwelling events.

region, a downwelling regime is present between May and November when the summer trade winds are replaced by the monsoonal winds advecting warm water (Fig. 3a) northward along the shore (Nykjaer and Van Camp, 1994). Our results (Fig. 2) are quite consistent with previous research (Nykjaer and Van Camp, 1994; Marcello et al., 2011; Santos et al., 2005, 2012; Cropper et al., 2014) but include the years 2010 to 2012, when the UI at around 20 – 21°N presented a shift of the upwelling intensity from high ($-2000 \text{ m}^2 \text{ s}^{-1}$) to strong ($-2800 \text{ m}^2 \text{ s}^{-1}$). The analysis of upwelling trends along this route has been controversial since it is highly dependent on the selected region (Santos et al., 2012). The interannual evolution of the UI over the period 2005 to 2012 (Fig. 4, green line) for each degree in latitude indicates an increase in the UI (mean confidence interval of $9 \text{ m}^2 \text{ s}^{-1}$) as showed by Santos et al. (2012).

North of 15°N , the upwelling index confirmed the stronger upwelling observed since 1995–1996 in this region after more than a 10-year (from at least 1982 to 1995) period of weaker upwelling (Santos et al., 2012). Local zonal differences between ocean and coastal SST trends determined with satellite data confirmed the intensification of the upwelling regime along the African coast for the period 1982 to 2000 (Santos et al., 2005) and extended by Santos et al. (2012) until 2010 and further extended in this study until 2012 (data not shown). This has been described as a decadal-scale shift of the upwelling regime intensity (Marcello et al., 2011; Santos et al., 2012).

South of 15°N , the annual UI values and trends (Figs. 2 and 4) both for the upwelling (values close to $-2800 \text{ m}^2 \text{ s}^{-1}$ in January) and downwelling (values reaching $1850 \text{ m}^2 \text{ s}^{-1}$ in July) periods are becoming stronger. At 11 – 12°N , where downwelling is becoming stronger, this results in negative annual temperature rates that approach zero. The UI serves as an indication of decadal variability of the summer monsoon winds and associated northward advection of warm water along the coast (Santos et al., 2012).

The highest upwelling intensity along the VOS line was located at the capes, Cap Blanc and Cap Vert. From satellite chlorophyll *a* data, especially off Cap Blanc, giant fila-

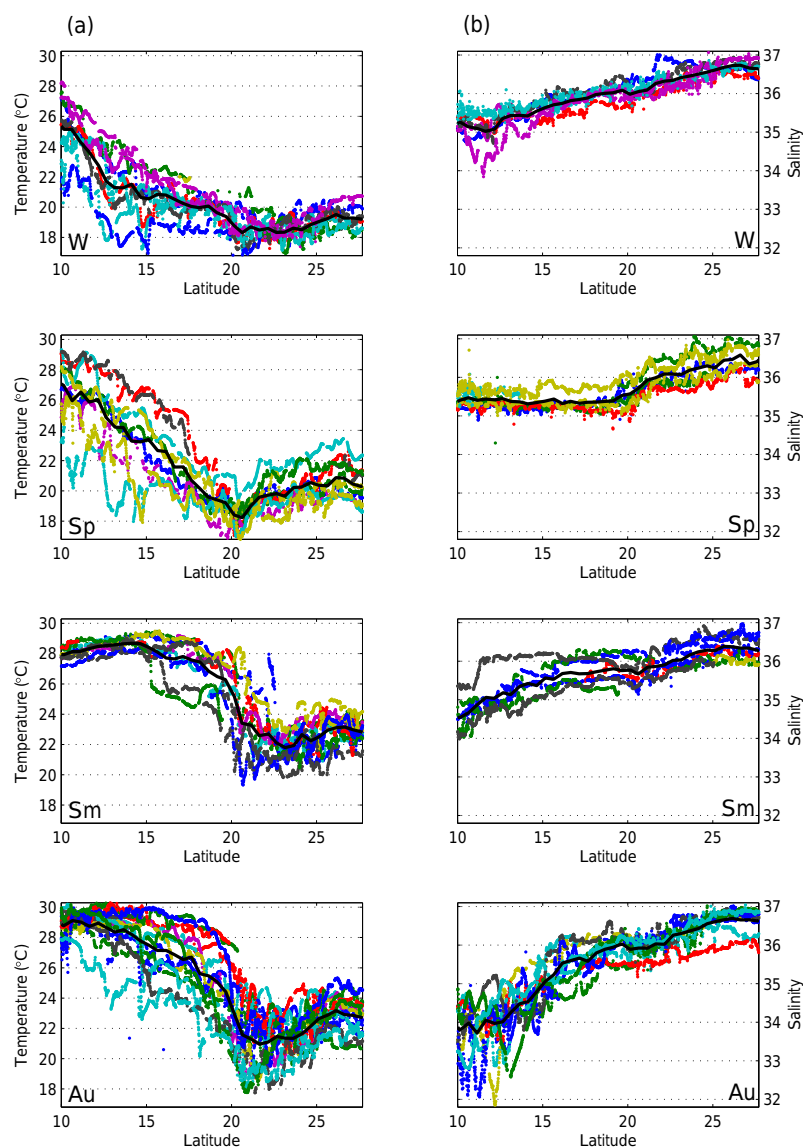


Figure 3. In situ data of column (a) SST and column (b) SSS in the Mauritanian–Cap Vert coastal region grouped by seasons: winter (W; December, January, and February), spring (Sp; March, April, and May), summer (Sm; June, July, and August), and autumn (Au; September, October, and November). The averaged values for all cruises in Table S1 are shown in black for each season including the 95 % confidence limits. The color code for each cruise is indicated in Table S1.

ments with chlorophyll concentrations above 1 mg m^{-3} persist year-round, spreading from the coast to several hundred kilometers offshore (Fig. 1). North of Cap Blanc the upwelled water originates from the North Atlantic Central Water, and mixes with South Atlantic Central Water (SACW) towards the south (Mittelstaedt, 1983). South of Cap Blanc, the upwelling of nutrient-rich SACW (Mittelstaedt, 1983) promotes phytoplankton growth between Cap Blanc and Cap Vert. Towards 12° N , upwelling is also fed by the North Equatorial Undercurrent (Hagen and Schemainda, 1984). Moreover, the entire northwest African coast is also influenced by the African desert dust transport by the mid-tropospheric Harmattan winds originating from the central

Sahara, which supplements the levels of micronutrients (such as iron) to the adjacent marine ecosystem (Mittelstaedt, 1983; Neuer et al., 2004).

The study area is also affected by the migration of the Intertropical Convergence Zone (ITCZ), related to maximum precipitation rates (Hastenrath, 1995). To have a significant satellite precipitation record in our region of interest, precipitation data were integrated longitudinally between 25.25 and 9.75° W . Time series for the latitudinal distribution of integrated precipitation (Fig. S1 in the Supplement) identified the average position of the ITCZ related to maximum precipitation rates. The ITCZ was located at its southernmost position (2° N) during winter, reaching its northernmost position

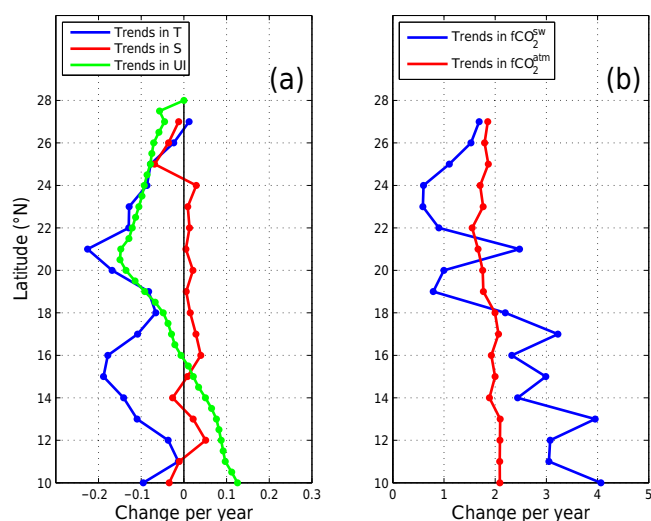


Figure 4. Latitudinal distribution of the interannual trends for the upwelling index (UI) and for the four experimental variables along the QUIMA-VOS line integrated over every degree between 2005 and 2012. Panel (a) presents the trends for upwelling index (UI, $\times 10^{-3} \text{ m}^2 \text{ s}^{-1}$, mean confidence interval of $9 \text{ m}^2 \text{ s}^{-1}$), SST ($^{\circ}\text{C yr}^{-1}$, confidence interval $0.13 ^{\circ}\text{C}$), and SSS (yr^{-1} , confidence interval 0.06) and (b) the trends for $f\text{CO}_2^{\text{sw}}$ and $f\text{CO}_2^{\text{atm}}$ (confidence intervals 4.23 and $0.44 \mu\text{atm}$).

($14\text{--}16^{\circ}\text{N}$) around summer. The ITCZ reached our area of interest ($> 10^{\circ}\text{N}$) from late spring to late summer.

The latitudinal distributions of measured SST and SSS along the vessel track are shown in Fig. 3, grouped by seasons (labeled W, Sp, Sm, and Au). The temperature generally decreased from 10°N to about $20\text{--}21^{\circ}\text{N}$, where the ship meets the Mauritanian upwelling. From there to the north, the temperature rises as the ship leaves the upwelling area on its way to the Canary Islands. In situ temperature at 27°N shows temperatures in the range of 18 to 24°C with the minimum in winter and maximum in late summer to early autumn. The annual temperature range was somewhat higher at 20°N , with a summer maximum of around 26°C and minimum in spring of about 17°C . At 10°N , temperatures were the highest throughout the year ($> 25^{\circ}\text{C}$), with minimum values in winter and maximum in late spring and late autumn. The low values observed during the end of summer are related to the arrival of the ITCZ (Fig. S1 in the Supplement) at those latitudes. The thermal distribution shows a temperature increase as we move to the Equator and a notable cooling at the upwelled waters off Mauritania. The upwelling of cold water from the Cap Vert area was only detected during winter time and the beginning of spring. Salinity minimum values were normally located at 10°N , increasing to maximum values at the Canaries' latitude. The minimum values of salinity were exceptionally low during autumn from 10 to 16°N by both the freshwater input from rivers that increase their outflow

during this season (Nicholson, 1981) and by the northward shift of the ITCZ during this time of the year.

Anomaly fields for temperature and salinity (data not shown) were calculated as the difference between the observations and the mean values at each season for individual latitudes. For temperature, the largest anomalies in winter and spring were located south of 18°N , with values of $\pm 2^{\circ}\text{C}$, related to the seasonal cycle of the Cap Vert upwelling. During summer the pattern changed and the largest anomalies were detected in the upwelling area at $18\text{--}22^{\circ}\text{N}$, with values of $\pm 5^{\circ}\text{C}$ when the upwelling index for the Mauritanian area was highest (Fig. 2). In autumn the temperature anomalies were shifted slightly to the north, $20\text{--}24^{\circ}\text{N}$, with values of $\pm 3^{\circ}\text{C}$ related to the observed pulses in upwelling-favorable winds that affected the surface seawater properties. On the other hand, salinity anomalies showed a very homogeneous pattern in all latitudes for winter, spring, and summer, with values generally within ± 0.5 . However, during autumn important anomalies south of 18°N were observed, with values in the range of ± 1.5 . In this region, the upwelling development, the river discharge, and the rainy season controlled the observed distribution (Yoo and Carton, 1990).

To conclude, the data show a permanent annual upwelling regime observed north of 20°N and a seasonal regime across $10\text{--}19^{\circ}\text{N}$, in accordance with the climatology of previous studies. The data also confirm an increase in upwelling conditions north of 20°N and an increase in downwelling conditions south of 20°N .

3.2 Carbon dioxide variability

The latitudinal distribution of the seasonal $f\text{CO}_2^{\text{sw}}$ data (Fig. 5a) showed the highest values between 18 and 23°N for all seasons due to the variability imposed by the upwelling off Mauritania. $f\text{CO}_2^{\text{sw}}$ was consistently greater than the $f\text{CO}_2^{\text{atm}}$. During winter, when the Cap Vert upwelling develops (Fig. 2), the $12\text{--}15^{\circ}\text{N}$ region also presented higher $f\text{CO}_2^{\text{sw}}$ values than those in the atmosphere. $f\text{CO}_2^{\text{sw}}$ data showed a latitudinal shift between the seasons following the shift observed in the upwelling index: in winter, the largest values were located between 19 and 24°N ; in spring, they were located between 16 and 22°N ; and during summer and autumn, the largest $f\text{CO}_2^{\text{sw}}$ values were recorded in the range 20 to 23°N . The difference between $f\text{CO}_2^{\text{sw}}$ normalized to the mean SST of 22°C for the region ($Nf\text{CO}_2^{\text{sw}}$) and $f\text{CO}_2^{\text{sw}}$ ($\Delta f\text{CO}_2 = Nf\text{CO}_2^{\text{sw}} - f\text{CO}_2^{\text{sw}}$, Fig. 5b) reinforced the variability at $20\text{--}23^{\circ}\text{N}$ all year around and at $12\text{--}17^{\circ}\text{N}$ during winter and spring, indicating that upwelling is the major factor contributing to the $f\text{CO}_2$ variability.

According to Takahashi et al. (1993), $f\text{CO}_2^{\text{sw}}$ increases with temperature at a rate of $4.3 \text{ \% } \mu\text{atm } ^{\circ}\text{C}^{-1}$ (between 15 and $26 \mu\text{atm } ^{\circ}\text{C}^{-1}$ in this area) in a thermodynamically controlled system. At 27°N , as SST increases, the rate was only $7.45 \mu\text{atm } ^{\circ}\text{C}^{-1}$ due mainly to biological uptake and also to CO_2 outflux. At 20°N the rate became negative with a value

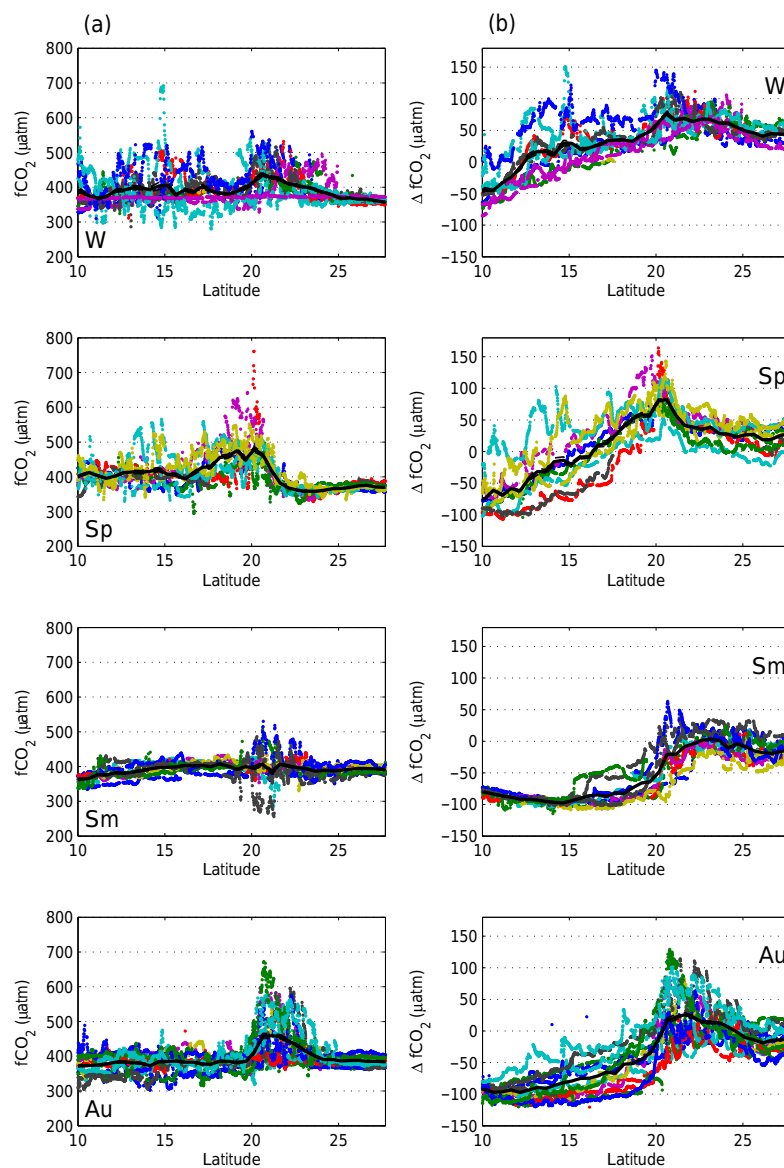


Figure 5. Fugacity of CO_2 data in the Mauritanian–Cap Vert coastal region grouped by seasons: winter (W; December, January, and February), spring (Sp; March, April, and May), summer (Sm; June, July, and August), and autumn (Au; September, October, and November). Column (a) $f\text{CO}_2^{\text{sw}}$ latitudinal distribution. Column (b), difference between measured and $f\text{CO}_2^{\text{sw}}$ values normalized to a constant temperature of 22°C . The averaged values for all cruises in Table S1 are shown in black for each season including the 95 % confidence limits. The color code for each cruise is indicated in Table S1.

of $-10.9 \mu\text{atm } ^\circ\text{C}^{-1}$, clearly indicating the important injection of cool and CO_2 -rich seawater at the upwelling area. The injection is not being compensated for by the solubility nor by the biological carbon pumps. At 10°N , the rate was still negative but only $-4.3 \mu\text{atm } ^\circ\text{C}^{-1}$ as a result of the seasonal upwelling. $\text{NfCO}_2^{\text{sw}}$ was related with SST (data not shown) in order to account for effects not removed during normalization. At latitudes 19 to 21°N , in the upwelling vicinity of Cap Blanc, an inverse relationship of $70\text{--}100 \mu\text{atm } ^\circ\text{C}^{-1}$ was found during winter and spring, while in summer and

autumn the inverse relationship rate was reduced to $12\text{--}18 \mu\text{atm } ^\circ\text{C}^{-1}$. While the upwelling indexes at those latitudes were quite constant throughout the year, different rates observed should be related to biological consumption of the CO_2 excess. However, during winter and spring the injection of CO_2 in the upwelling is not decreased by the biological activity in the area. But during the Chlorophyll *a* maximum (late spring and summer), most of the CO_2 was consumed and/or exported and, therefore, the rate was strongly reduced.

Figure 4 depicts the observed interannual trends (a_1 coefficient in Eq. 4) for the four experimentally recorded detrended parameters, together with the UI trend. Confidence intervals of the computed mean annual values for SST, SSS, $f\text{CO}_2^{\text{atm}}$, and $f\text{CO}_2^{\text{sw}}$ were 0.13°C , 0.06 , 0.44 , and $4.23\ \mu\text{atm}$, respectively. There was a clear SST trend whereby seawater along the VOS line track was getting cooler with maximum cooling rates at the location of Cap Blanc (21°N) and Cap Vert upwellings (15°N) with rates higher than $-0.2^\circ\text{C yr}^{-1}$. Data from the first 3 years (2005 to 2008) at 21°N showed lower temperatures with higher cooling rates that reached $-0.7^\circ\text{C yr}^{-1}$, although 3 years of data are not representative. The area crossed by the VOS line along $17^\circ45'\text{W}$ from 22 to 10°N is located inside the 1000 m isobath that is well inside the mean frontal activity in the Canary region, about 200 km wide (Wang et al., 2015). The different changes in temperature in the coastal slope and offshore waters are related to the different origins of the waters upwelled from depths of about 100 m to the surface (Mittelstaedt, 1983) that spread off the coastal area. The offshore water SST is less variable owing to longer residence time in the ocean surface. These effects and the fact that the VOS line keeps a track line that crossed the upwelling cells at a distance to the coast that varies among cells contribute to the observed spatial variability. There was no attempt to compare latitudinal and longitudinal effects on the observed values. Our experimental data, however, do not show any positive SST rates in the upwelling affected area, and only when the ship approached the Canary Islands did the trends become less negative, reaching a value of $+0.02^\circ\text{C yr}^{-1}$ at 27°N , similar to those obtained for oceanic Atlantic water (Bates et al., 2014).

$f\text{CO}_2^{\text{atm}}$ for the area showed the interannual increase of about $2 \pm 0.3\ \mu\text{atm yr}^{-1}$ observed in atmospheric stations, while $f\text{CO}_2^{\text{sw}}$ presented a heterogeneous distribution. South of 18°N , the rate of increase was always higher than that in the atmosphere reaching a maximum value of $4.1 \pm 0.4\ \mu\text{atm yr}^{-1}$ at 10°N . At 27°N , $f\text{CO}_2^{\text{sw}}$ increased at a rate of $1.7 \pm 0.2\ \mu\text{atm yr}^{-1}$ similar to that determined at the ESTOC time series site (González-Dávila et al., 2010) located at $29^\circ10'\text{N}$, $15^\circ30'\text{W}$. In the Cap Blanc area, $f\text{CO}_2^{\text{sw}}$ increased at an average rate of $2.5 \pm 0.4\ \mu\text{atm yr}^{-1}$ with the highest values in the period 2005 to 2008 (a rate of $4.6 \pm 0.5\ \mu\text{atm yr}^{-1}$ was computed with only those years). Around Cap Blanc, $f\text{CO}_2^{\text{sw}}$ always presented lower rates of increase than in the atmosphere with values well below $1\ \mu\text{atm yr}^{-1}$. The observed decrease in SST and the trends in $f\text{CO}_2^{\text{sw}}$ can only be explained by a reinforced upwelling. North of 18°N , the lowest rate of increase in $f\text{CO}_2^{\text{sw}}$ compared to $f\text{CO}_2^{\text{atm}}$, together with a decrease in temperature, indicated that upwelling is also favoring an increase in the net community production around the Mauritanian upwelling, consuming and/or exporting the CO_2 -rich upwelled waters favored by the lateral transport of the Mauritanian current (Lachkar and Gruber, 2013; Varela et al., 2015). The

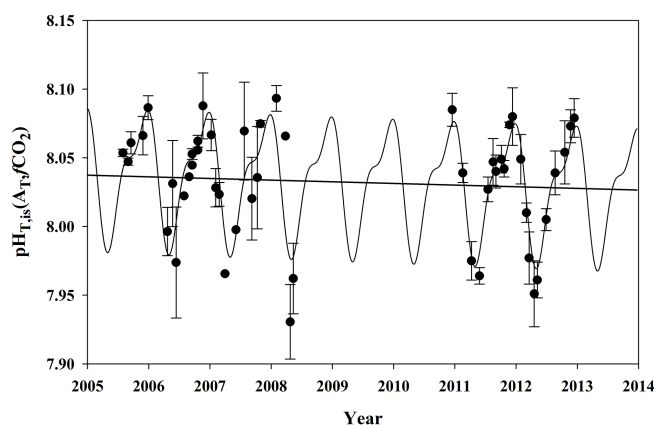


Figure 6. pH of surface waters in total proton scale and at in situ SST computed from total alkalinity (based on regional correlations with SST and SSS; Lee et al., 2006) and $f\text{CO}_2$ at $21 \pm 0.25^\circ\text{N}$. The error bars represent the standard deviation of the computed data for each cruise for the selected latitude. The black curve shows the harmonic fitting of Eq. (4) for the data and the corresponding linear trend is also shown.

upwelling intensification effects observed in the trends of our experimental data support the recent wind stress trends (Cropper et al., 2014; Varela et al., 2015; Santos et al., 2012) of increased upwelling-favorable winds, at least for the period 2005–2012 in the Canary upwelling region (Figs. 2 and 4). The intensification of the upwelling results in a change in the measured upwelled water properties due to either higher upwelling velocities or deeper source upwelled waters. However, what remains unclear from these records is to what extent those changes reflect upwelling variations due to climate change forcing versus natural decadal variability in the upwelling areas occurring over interannual timescales.

Because the upwelling intensity is changing, other variables will also be affected. $\text{pH}_{T, \text{is}}$ at $21 \pm 0.25^\circ\text{N}$ was computed from $f\text{CO}_2$ and alkalinity pairs of data. Alkalinity was computed from regional correlations with SST and SSS (Lee et al., 2006), which could underrepresent seasonal and interannual variations in upwelling areas. However, pH computed from $f\text{CO}_2$ values are relatively insensitive to errors in A_T , and $f\text{CO}_2$ controls the magnitude and variability of pH (a $60\ \mu\text{mol kg}^{-1}$ change in A_T will affect a 0.1 % in pH, that is, about 0.01 pH units). Figure 6 depicts the computed $\text{pH}_{T, \text{is}}$ (A_T , $f\text{CO}_2$) data and the harmonic fitting of Eq. (4) providing the seasonal variability and interannual trend. Considering the small systematic biases in interannual dynamics, we determined a decrease in pH at a rate of $-0.003 \pm 0.001\ \text{yr}^{-1}$ (Fig. 6). This decrease is one of the highest rate values determined in several time series stations (Bates et al., 2014), where oceanic SST has only slightly increased in the last decades. However, at the Mauritanian upwelling area and at the location where our VOS line approached this region, SST decreased at a rate of $-0.22 \pm 0.06^\circ\text{C yr}^{-1}$ (Fig. 4). Solely

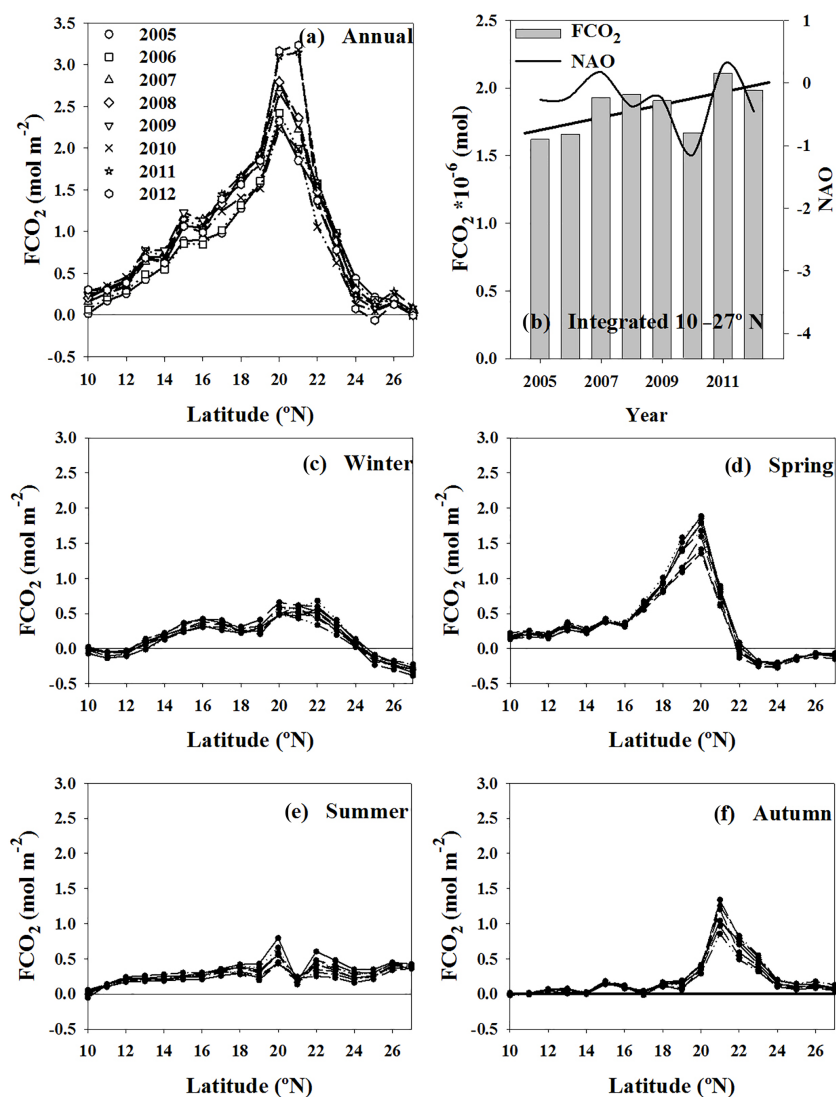


Figure 7. Latitudinal distributions of seasonal and annual CO₂ fluxes (FCO₂, mol m⁻²). Fluxes of CO₂ were computed using Nightingale et al. (2000) parameterization and satellite winds with a resolution of 6 h. **(a)** Integrated year to year from 2005 to 2012 and **(b)** latitudinally integrated for 2005 to 2012 together with annual values for the North Atlantic Oscillation (NAO) index. Latitudinal distributions of FCO₂ seasonally integrated from 2005 to 2012 are depicted for **(c)** winter (December, January, and February), **(d)** spring (March, April, and May), and **(e)** summer (June, July, and August).

this decrease in temperature would increase the pH by a rate of $+0.004 \text{ yr}^{-1}$ and the $f\text{CO}_2$ would decrease by $4 \mu\text{atm yr}^{-1}$. The net effect of the increase in the amount of rich CO₂ and lower pH upwelled waters in the Mauritanian upwelling would be, therefore, a decrease in the pH rate of over $-0.007 \pm 0.002 \text{ units yr}^{-1}$ and an increase in $f\text{CO}_2$ of $+6.5 \pm 0.7 \mu\text{atm yr}^{-1}$ (with periods where those rates could reach values of -0.015 yr^{-1} in pH and $+10.5 \mu\text{atm yr}^{-1}$ in $f\text{CO}_2$ as recorded during 2005–2008). Those values are greatly compensated for by the important decrease in the SST resulting in the determined rates of $-0.003 \pm 0.001 \text{ pH units}$ and $+2.5 \pm 0.4 \mu\text{atm}$ of $f\text{CO}_2$ per year.

This new data set of experimental values confirmed a decrease in SST and trends in $f\text{CO}_2^{\text{sw}}$ that can only be explained by reinforced upwelling conditions that favor an increase in the net community production around the Mauritanian upwelling together with a more corrosive environment with pH rates that change by more than $-0.007 \pm 0.002 \text{ yr}^{-1}$ at 21° N. However, the decrease in SST in the upwelling cell buffers this pH rate to values around $-0.003 \pm 0.001 \text{ yr}^{-1}$ and $+2.5 \pm 0.4 \mu\text{atm yr}^{-1}$ in $f\text{CO}_2$, still among the highest observed in other time series.

3.3 Fluxes of CO₂

The annual air–sea CO₂ flux for the full domain was positive (Fig. 7a), with the area off Cap Blanc with values close to 3.3 mol CO₂ m^{−2} (Fig. 7a). North of 24° N, in the area not affected by the coastal upwelling, an average flux of $+0.14 \pm 0.03$ mol CO₂ m^{−2} was determined. The ingassing observed during winter and spring of -0.16 ± 0.03 mol CO₂ m^{−2} for the full period (Fig. 7) was surpassed by the outgassing during summer and autumn of 0.28 ± 0.14 mol CO₂ m^{−2}. South of 24° N, it was observed that during spring (Fig. 7d) the photosynthetic activity was not intense enough to uptake the CO₂ injected by the strongest upwelling in the surface waters and thus the area acted as a source of CO₂ with values reaching 1.9 mol CO₂ m^{−2} in 2012. During summer (Fig. 7e), primary producers and lateral advection of warm waters by the Mauritanian current could consume and/or export the CO₂-rich waters reaching values of 0.5 mol CO₂ m^{−2}. During autumn (Fig. 7f), only the area between 20 and 23° N acted as a source of 1–1.5 mol CO₂ m^{−2}, while the rest was almost in equilibrium. Late autumn–winter upwelling in the 14 to 17° N region contributed to an increased outgassing with a second annual submaximum of about 0.4 mol CO₂ m^{−2} in winter (Fig. 7c). South of 14° N, annual CO₂ fluxes decreased from about 0.7 mol CO₂ m^{−2} at 14° N to being roughly in equilibrium at 10° N.

The integrated CO₂ fluxes for the area between 10 and 27° N along the VOS line section for the years 2005 to 2012 (Fig. 7b) were between 1.6 and 2.1×10^6 mol of CO₂, with an important annual variability. FCO₂ increased during the studied period by $0.05 \pm 0.02 \times 10^6$ mol yr^{−1}. The increase in FCO₂ is related to the observed increase in wind speed (Fig. 4, indicated as UI) north of 16° N. North of 19° N, the influence of wind speed far surpassed the effect of the smaller annual rate of increase in $f\text{CO}_2^{\text{sw}}$ relative to $f\text{CO}_2^{\text{atm}}$, with an exception at 21° N (Fig. 4). South of 16° N, the decrease in wind speed did not exceed the effect of the incremental change in $(f\text{CO}_2^{\text{sw}} - f\text{CO}_2^{\text{atm}})$ associated with the increased downwelling indexes (Fig. 4; Santos et al., 2012), resulting in a slightly increasing FCO₂. The variability observed in the annual integrated CO₂ fluxes (Fig. 7b) was related with the basin-scale oscillations, the North Atlantic Oscillation (NAO) index and the east Atlantic pattern (EA) (<http://www.cpc.ncep.noaa.gov/data/teledoc/telecontents.shtml>). Cropper et al. (2014) found winter upwelling variability was strongly correlated with the winter NAO (r values ranged from 0.50 at 12–19° N to 0.59 at 21–26° N), due to the influence of the Azores semi-permanent high-pressure system on the strength of the trade winds. The annual integrated FCO₂ was related with the annual NAO index (Fig. 7b) with a similar $r = 0.54$, even when fluxes are not only controlled by wind strength. However, Fig. 7a clearly indicates that the Mauritanian upwelling area was the most important contributor to FCO₂ in the study

area. The FCO₂ was not significantly correlated with the winter NAO ($r = 0.23$). Also, the EA index, which represents a southward-shifted NAO-like oscillation, presented a lower significant value ($r = 0.48$) (trends not shown), in agreement with the upwelling index (Cropper et al., 2014). Overall, the correlation between fluxes and climate indexes describing the main mode of variability across the Atlantic sector may be directly related to the Azores High and its influence on the trade wind strength.

FCO₂ values along the QUIMA-VOS line were used in order to compute a flux budget for the Mauritanian–Cap Vert region. The observed values were assumed to be valid for at least 100 km on both sides of the QUIMA-VOS line. In this case, the total flux of CO₂ being ejected to the atmosphere would reach a value of 16 Tg of carbon dioxide a year for the period 2005–2012, with a rate of increase of $+0.6$ Tg yr^{−1}. However, it should be considered that the export of the rich $f\text{CO}_2$ upwelled water with high nutrient concentration off the coastal areas would promote a decrease in surface $f\text{CO}_2$ values during productive seasons (as those observed north and south of 21° N) that will result in an ingassing of CO₂. This could balance the observed outgassing increase on a more global scale.

4 Conclusions

The Mauritanian–Cap Vert upwelling area's sensitivity to climatic forcing on upwelling processes strongly affects the CO₂ surface distribution, ocean acidification rates, and air–sea CO₂ exchange.

The experimental SST and carbon dioxide system variable results for the period 2005 to 2012 confirm upwelling intensification at the Mauritanian–Cap Vert upwelling system. Furthermore, we have shown that upwelling regions at low to midlatitudes are important sources of CO₂ for the atmosphere. As a direct result, the pH is decreasing at a rate of -0.003 ± 0.001 yr^{−1}. Importantly, the amount of emitted CO₂ is increasing annually at a rate of 0.6 Tg due to stronger wind stress, even when primary production seems to also be enhanced in the upwelling area. The monthly record in this EBUS is not yet long enough to determine the extent to which these changes can be attributed to natural decadal variability. These VOS lines must be maintained for years to come and will continue to be one of the most significant contributors to our knowledge of how ocean surface waters are being affected by present and future climate change. The results from VOS lines can provide accurate data for changes in SST, FCO₂, and, consequently, upwelling intensification effects due to global change conditions under decadal natural variability.

Data availability. All data are freely available at the SOCAT database, <http://www.socat.info/> (Pfeil et al., 2013), and at the CAR-

BOOCEAN and CARBOCHANGE web pages, www.CarboOcean.org and <https://carbochange.b.uib.no/>, respectively.

The Supplement related to this article is available online at <https://doi.org/10.5194/bg-14-3859-2017-supplement>.

Author contributions. MGD and JMSC worked in the equipment installation, data collection and designed the study. FM processed the data and generated figures and results. All of them collaborated in the discussion of the data and the writing of the paper.

Competing interests. The authors declare that they have no conflict of interest.

Special issue statement. This article is part of the special issue “The Ocean in a High-CO₂ World IV”. It is a result of the 4th International Symposium on the Ocean in a High-CO₂ World, Hobart, Australia, 3–6 May 2016.

Acknowledgements. Financial support from the European Union through the integrated project FP6 CARBOOCEAN under grant agreement no. 511106-2, FP7 project CARBOCHANGE under grant agreement no. 264879 and H2020 project ATLANTOS under agreement no. 633211 is gratefully acknowledged. Special thanks go to the Mediterranean Shipping Company (MSC) (years 2005–2008) and Maersk (years 2010–2013), who provided the ship platforms and scientific facilities. We thank April Abbott (Macquarie University, Sydney) for her comments and English correction. The MODIS-Aqua Ocean Color Data, 2005–2012 reprocessing, NASA OB.DAAC, Greenbelt, MD, USA, is strongly acknowledged.

Edited by: Kai G. Schulz

Reviewed by: two anonymous referees

References

- Astor, Y., Scranton, M., Muller-Karger, F., Bohrer, R. N., and Garcia, J.: CO₂ variability at the CARIACO tropical coastal upwelling time series station, *Mar. Chem.*, 97, 245–261, 2005.
- Bakun, A.: Global climate change and intensification of coastal ocean upwelling, *Science*, 247, 198–201, 1990.
- Barton, E. D., Field, D. B., and Roy, C.: Canary current upwelling: More or less?, *Prog. Oceanogr.*, 116, 167–178, 2013.
- Bates, N. R., Astor, Y. M., Church, M. J., Currie, K., Dore, J. E., González-Dávila, M., Lorenzoni, L., Muller-Karger, F., Olafsson, J., and Santana-Casiano, J. M.: A time-series view of changing ocean chemistry due to ocean uptake of anthropogenic CO₂ and ocean acidification, *Oceanography*, 27, 126–141, <https://doi.org/10.5670/oceanog.2014.16>, 2014.
- Borges, A. V. and Frankignoulle, M.: Distribution of surface carbon dioxide and air-sea exchange in the upwelling system off the Galician coast, *Global Biogeochem. Cy.*, 16, 1020, <https://doi.org/10.1029/2000GB001385>, 2002.
- Borges, A. V., Delille, B., and Frankignoulle, M.: Budgeting sinks and sources of CO₂ in the coastal ocean: Diversity of ecosystems counts, *Geophys. Res. Lett.*, 32, L14601, <https://doi.org/10.1029/2005GL023053>, 2005.
- Cai, W.-J., Dai, M., and Wang, Y.: Air–sea exchange of carbon dioxide in ocean margins: a province-based synthesis, *Geophys. Res. Lett.*, 33, L12603, <https://doi.org/10.1029/2006GL026219>, 2006.
- Chen, C.-T. A., Huang, T.-H., Chen, Y.-C., Bai, Y., He, X., and Kang, Y.: Air–sea exchanges of CO₂ in the world’s coastal seas, *Biogeosciences*, 10, 6509–6544, <https://doi.org/10.5194/bg-10-6509-2013>, 2013.
- Cropper, T. E., Hanna, E., and Bigg, G. R.: Spatial and temporal seasonal trends in coastal upwelling off Northwest Africa, 1981–2012, *Deep-Sea Res. Pt. I*, 86, 94–111, 2014.
- Demarcq, H.: Trends in primary production, sea surface temperature and wind in upwelling systems (1998–2007), *Prog. Oceanogr.*, 83, 376–385, <https://doi.org/10.1016/j.pocan.2009.07.022>, 2009.
- Dickson, A. G. and Millero, F. J.: A comparison of the equilibrium constants for the dissociation of carbonic acid in seawater media, *Deep-Sea Res.*, 34, 1733–1743, 1987.
- DOE: Handbook of methods for the analysis of the various parameters of the carbon dioxide system in sea water, ORNL/CDIAC-74, available at: <http://cdiac.ornl.gov/oceans/handbook.html> (last access: 7 March 2017), 1994.
- Dore, J. E., Lukas, R., Sadler, D. W., and Karl, D. M.: Climate-driven changes to the atmospheric CO₂ sink in the subtropical North Pacific Ocean, *Nature*, 424, 754–757, 2003.
- Feely, R. A., Boutin, J., Cosca, C. E., Dandonneau, Y., Etcheto, J., Inoue, H. Y., Ishii, M., Quéré, C. L., Mackey, D. J., McPhaden, M., Metzl, N., Poisson, A., and Wanninkhof, R.: Seasonal and interannual variability of CO₂ in the equatorial Pacific, *Deep Sea Res. Pt. II*, 49, 2443–2469, 2002.
- Feely, R. A., Sabine, C. L., Hernandez-Ayon, J. M., Ianson, D., and Hales, B.: Evidence for upwelling of corrosive “acidified” water onto the continental shelf, *Science*, 320, 1490–1492, <https://doi.org/10.1126/science.1155676>, 2008.
- Frankignoulle, M. and Borges, A. V.: European continental shelf as a significant sink for atmospheric carbon dioxide, *Global Biogeochem. Cy.*, 15, 569–576, 2001.
- Friederich, G. E., Ledesma, J., Ulloa, O., and Chavez, F. P.: Air-sea carbon dioxide fluxes in the coastal southeastern tropical Pacific, *Prog. Oceanogr.*, 79, 156–166, 2008.
- González Dávila, M., Santana-Casiano, M. J., Merlivat, L., Barbero-Munoz, L., and Dafner, E.: Fluxes of CO₂ between the atmosphere and the ocean during the POMME project in the northeast Atlantic Ocean during 2001, *J. Geophys. Res.*, 110, C07S11, <https://doi.org/10.1029/2004JC002763>, 2005.
- González-Dávila, M., Santana-Casiano, J. M., and Ucha, I.: Seasonal variability of fCO₂ in the Angola-Benguela region, *Prog. Oceanogr.*, 83, 124–133, 2009.
- González-Dávila, M., Santana-Casiano, J. M., Rueda, M. J., and Llinás, O.: The water column distribution of carbonate system variables at the ESTOC site from 1995 to 2004, *Biogeosciences*, 7, 3067–3081, <https://doi.org/10.5194/bg-7-3067-2010>, 2010.

- Gruber, N.: Warming up, turning sour, losing breath: ocean biogeochemistry under global change, *Philos. T. R. Soc. Lond.*, 369, 1980–1996, 2011.
- Gruber, N., Keeling, C. D., and Bates, N. R.: Interannual variability in the North Atlantic Ocean carbon sink, *Science*, 298, 2374–2378, 2002.
- Hagen, E. and Schemainda, R.: Der Guineadom im ostatlantischen Stromsystem, *Beitr. Meereskd.*, 51, 5–27, 1984.
- Hales, B., Takahashi, T., and Bandstra, L.: Atmospheric CO₂ uptake by a coastal upwelling system, *Global Biogeochem. Cy.*, 19, GB1009, <https://doi.org/10.1029/2004GB002295>, 2005.
- Hastenrath, S.: *Climate Dynamics of the Tropics*, 488 pp., Kluwer Acad., Norwell, Mass., 1995.
- Keeling, R. F., Kortzinger, A., and Gruber, N.: Ocean deoxygenation in a warming world, *Annu. Rev. Mar. Sci.*, 2, 199–229, <https://doi.org/10.1146/annurev.marine.010908.163855>, 2010.
- Key, R., Kozyr, A., Sabine, C., Lee, K., Wanninkhof, R., Bullister, J., Feely, R., Millero, F. J., Mordy, C., and Peng, T.-H.: A global ocean carbon climatology: Results from GLODAP, *Global Biogeochem. Cy.*, 18, GB4031, <https://doi.org/10.1029/2004GB002247>, 2004.
- Lachkar, Z. and Gruber, N.: Response of biological production and air–sea CO₂ fluxes to upwelling intensification in the California and Canary Current Systems, *J. Marine Syst.*, 109–110, 149–160, 2013.
- Lee, K., Tong, L. T., Millero, F. J., Sabine, C. L., Dickson, A. G., Goyet, C., Park, G. H., Wanninkhof, R., Feely, R. A., and Key, R. M.: Global relationships of total alkalinity with salinity and temperature in surface waters of the world's oceans, *Geophys. Res. Lett.*, 33, L19605, <https://doi.org/10.1029/2006GL027207>, 2006.
- Lüger, H., Wallace, D. W., Kortzinger, A., and Nojiri, Y.: The pCO₂ variability in the midlatitude North Atlantic Ocean during a full annual cycle, *Global Biogeochem. Cy.*, 18, GB3023, <https://doi.org/10.1029/2003GB002200>, 2004.
- Lüger, H., Wanninkhof, R., Wallace, D. W., and Kortzinger, A.: CO₂ fluxes in the subtropical and subarctic North Atlantic based on measurements from a volunteer observing ship, *J. Geophys. Res.*, 111, C06024, <https://doi.org/10.1029/2005JC003101>, 2006.
- Marcello, J., Alonso, H., Eugenio, F., and Fonte, A.: Seasonal and temporal study of the northwest African upwelling system, *Int. J. Remote Sens.*, 32, 1843–1859, <https://doi.org/10.1080/01431161003631576>, 2011.
- Mehrbach, C., Culbertson, C. H., Hawley, J. E., and Pytkowicz, R. N.: Measurement of the apparent dissociation constants of carbonic acid in seawater at atmospheric pressure, *Limnol. Oceanogr.*, 18, 897–907, 1973.
- Michaels, A. F., Karl, D. M., and Capone, D. G.: Element stoichiometry, new production and nitrogen fixation, *Oceanography*, 14, 68–77, 2001.
- Mittelstaedt, E.: The upwelling area off Africa – A description of phenomena related to coastal upwelling, *Prog. Oceanogr.*, 12, 307–331, [https://doi.org/10.1016/0079-6611\(83\)90012-5](https://doi.org/10.1016/0079-6611(83)90012-5), 1983.
- Neuer, S., Torres-Padrón, M. E., Gelado-Caballero, M. D., Rueda, M. J., Hernández-Brito, J. J., Davenport, R., and Wefer, G.: Dust deposition pulses to the eastern subtropical North Atlantic gyre: Does ocean's biogeochemistry respond?, *Global Biogeochem. Cy.*, 18, GB4020, <https://doi.org/10.1029/2004GB002228>, 2004.
- Nicholson, S. E.: Rainfall and atmospheric circulation during drought periods and wetter years in West Africa, *Mon. Weather Rev.*, 109, 2191–2208, 1981.
- Nightingale, P. D., Malin, G., Law, C. S., Watson, A. J., Liss, P. S., Liddicoat, M. L., Boutin, J., and Upstill-Goddard, R. C.: In situ evaluation of air–sea gas exchange parameterizations using novel conservative and volatile tracers, *Global. Biogeochem. Cy.*, 14, 373–387, 2000.
- Nykjaer, L. and Van Camp, L.: Seasonal and interannual variability of coastal upwelling along Northwest Africa and Portugal from 1981 to 1991, *J. Geophys. Res.*, 99, 14197–14207, 1994.
- Oerder, V., Colas, F., Echevin, V., Codron, F., Tam, J., and Belmadani, A.: Peru–Chile upwelling dynamics under climate change, *J. Geophys. Res.-Oceans*, 120, 1152–1172, <https://doi.org/10.1002/2014JC010299>, 2015.
- Padin, X. A., Vázquez-Rodríguez, M., Castaño, M., Velo, A., Alonso-Pérez, F., Gago, J., Gilcoto, M., Álvarez, M., Pardo, P. C., de la Paz, M., Ríos, A. F., and Pérez, F. F.: Air–Sea CO₂ fluxes in the Atlantic as measured during boreal spring and autumn, *Biogeosciences*, 7, 1587–1606, <https://doi.org/10.5194/bg-7-1587-2010>, 2010.
- Pfeil, B., Olsen, A., Bakker, D. C. E., Hankin, S., Koyuk, H., Kozyr, A., Malczyk, J., Manke, A., Metzl, N., Sabine, C. L., Akl, J., Alin, S. R., Bates, N., Bellerby, R. G. J., Borges, A., Boutin, J., Brown, P. J., Cai, W.-J., Chavez, F. P., Chen, A., Cosca, C., Fassbender, A. J., Feely, R. A., González-Dávila, M., Goyet, C., Hales, B., Hardman-Mountford, N., Heinze, C., Hood, M., Hoppema, M., Hunt, C. W., Hydes, D., Ishii, M., Johannessen, T., Jones, S. D., Key, R. M., Kortzinger, A., Landschützer, P., Lauvset, S. K., Lefèvre, N., Lenton, A., Lourantou, A., Merlivat, L., Midorikawa, T., Mintrop, L., Miyazaki, C., Murata, A., Nakadate, A., Nakano, Y., Nakaoka, S., Nojiri, Y., Omar, A. M., Padin, X. A., Park, G.-H., Paterson, K., Perez, F. F., Pierrot, D., Poisson, A., Ríos, A. F., Santana-Casiano, J. M., Salisbury, J., Sarma, V. V. S. S., Schlitzer, R., Schneider, B., Schuster, U., Sieger, R., Skjelvan, I., Steinhoff, T., Suzuki, T., Takahashi, T., Tedesco, K., Telszewski, M., Thomas, H., Tilbrook, B., Tjiputra, J., Vandemark, D., Veness, T., Wanninkhof, R., Watson, A. J., Weiss, R., Wong, C. S., and Yoshikawa-Inoue, H.: A uniform, quality controlled Surface Ocean CO₂ Atlas (SOCAT), *Earth Syst. Sci. Data*, 5, 125–143, <https://doi.org/10.5194/essd-5-125-2013>, 2013.
- Santana-Casiano, J., González-Dávila, M., and Ucha, I.: Carbon dioxide fluxes in the Benguela upwelling system during winter and spring: A comparison between 2005 and 2006, *Deep-Sea Res. Pt. II*, 56, 533–541, 2009.
- Santana-Casiano, J. M., González-Dávila, M., Rueda, M., Llinás, O., and González-Dávila, E.-F.: The interannual variability of oceanic CO₂ parameters in the northeast Atlantic subtropical gyre at the ESTOC site, *Global Biogeochem. Cy.*, 21, GB1015, <https://doi.org/10.1029/2006GB002788>, 2007.
- Santos, A. M. P., Kazmin, A. S., and Peliz, A.: Decadal changes in the Canary upwelling system as revealed by satellite observations: Their impact on productivity, *J. Mar. Res.*, 63, 359–379, 2005.
- Santos, F., de Castro, M., Gómez-Gesteira, M., and Alvarez, I.: Differences in coastal and oceanic SST warming rates along the Canary upwelling ecosystem from 1982 to 2010, *Cont. Shelf Res.*, 47, 1–6, 2012.

- Schuster, U., Watson, A., Bates, N., Corbiere, A., Gonzalez-Davila, M., Metzl, N., Pierrot, D., and Santana-Casiano, J. M.: Trends in North Atlantic sea-surface $f\text{CO}_2$ from 1990 to 2006, *Deep-Sea Res. Pt. II*, 56, 620–629, 2009.
- Takahashi, T., Olafsson, J., Goddard, J. G., Chipman, D. W., and Sutherland, S.: Seasonal variation of CO_2 and nutrients in the high-latitude surface oceans: A comparative study, *Glob. Biogeochem. Cy.*, 7, 843–878, 1993.
- Takahashi, T., Sutherland, S., Wanninkhof, R., Sweeney, C., Feely, R., Chipman, D., Hales, B., Friederich, G., Chavez, F., Sabine, C., Watson, A., Bakker, D., Schuster, U., Metzl, N., Yoshikawa-Inoue, H., Ishii, M., Midorikawa, T., Nojiri, Y., Kortzinger, A., Steinhoff, T., Hoppema, M., Olafsson, J., Arnarson, T., Tilbrook, B., Johannessen, T., Olsen, A., Bellerby, A., Wong, C., Delille, B., Bates, N., and de Baar, H.: Climatological mean and decadal change in surface ocean pCO_2 , and net sea-air CO_2 flux over the global oceans, *Deep-Sea Res. Pt. II*, 56, 554–577, 2009.
- Ullman, D. J., McKinley, G. A., Bennington, V., and Dutkiewicz, S.: Trends in the North Atlantic carbon sink: 1992–2006, *Glob. Biogeochem. Cy.*, 23, GB4011, <https://doi.org/10.1029/2008GB003383>, 2009.
- Varela, R., Álvarez, I., Santos, F., de Castro, M., and Gómez-Gesteira, M.: Has upwelling strengthened along worldwide over 1982–2010?, *Sci. Rep.*, 5, 10016, <https://doi.org/10.1038/srep10016>, 2015.
- Wang, Y., Castelao, R. M., and Yuan, Y.: Seasonal variability of alongshore winds and sea surface temperature fronts in Eastern Boundary Current Systems, *J. Geophys. Res.-Oceans*, 120, 2385–2400, <https://doi.org/10.1002/2014JC010379>, 2015.
- Watson, A., Schuster, U., Bakker, D., Bates, N., Corbière, A., González-Dávila, M., Friedrich, T., Hauck, J., Heinze, C., Johannessen, T., Kortzinger, A., Metzl, N., Olafsson, J., Olsen, A., Oschlies, A., Padin, X. A., Pfeil, B., Santana-Casiano, J. M., Steinhoff, T., Telszewski, M., Rios, A. F., Wallace, D. W., and Wanninkhof, R.: Tracking the variable North Atlantic sink for atmospheric CO_2 , *Science*, 326, 1391–1393, <https://doi.org/10.1126/science.1177394>, 2009.
- Yoo, J.-M. and Carton, J. A.: Annual and interannual variation of the freshwater budget in the tropical Atlantic Ocean and the Caribbean Sea, *J. Phys. Oceanogr.*, 20, 831–845, 1990.

Reproduced with permission of copyright owner.
Further reproduction prohibited without permission.